



Flow Field and Heat Transfer Investigation of a Confined Laminar Slot Air Jet on a Solid Block

M. Muthukannan^{1†}, P. Rajesh Kanna², S. Jeyakumar¹ and A. Bajpai³

¹ Kalasalingam University, Krishnankoil, Tamilnadu, 626126, India

² Velammal College of Engineering and Technology, Madurai, Tamilnadu-625009, India

³ Department of Aerospace Engineering, IISc, Bangalore, India

†Corresponding Author Email: mmk.mech59@gmail.com

(Received December 12, 2015; accepted September 20, 2015)

ABSTRACT

A numerical investigation is carried out to investigate the fluid flow field and heat transfer characteristics of two dimensional laminar incompressible jet flows. Simulations are performed for a single vertical slot jet on a block mounted on the bottom wall and the top wall is confined by a parallel wall surface. The present study reveals the vital impact of the Aspect Ratio (AR) and Reynolds number (Re) on the fluid flow and heat transfer characteristics over a wide range. It is observed that the presence of a solid block in the channel increases the overall unsteadiness in the flow. The correlation between the Reynolds numbers and reattachment length is suggested, for all Aspect Ratios (ARs). The horizontal velocity profile at various downstream locations for all ARs is employed to find out the location where the flow gets fully developed. The primary peak value of the Nusselt number (Nu) occurs at the stagnation point, and the secondary peak is at a downstream location. The average Nusselt number increases with the increase of Reynolds number and decreases with the increase of the distance between the jet and the block. The heat transfer correlations between the Reynolds number and Nusselt number are analyzed for constant wall temperature boundary conditions.

Keywords: Impinging jet; Reynolds number; Aspect Ratio; Nusselt Number; Vortex center; Coefficient of friction.

NOMENCLATURE

AR	Aspect Ratio of the domain	U, V	dimensionless velocity components
AV	Adjacent Vortex	W	width of the jet.
C _f	skin friction coefficient	W/D _h	dimensionless jet width
D _h	hydraulic diameter of the jet	x	space coordinates in m
L _x	length of the computational domain in the X direction	y	space coordinates in m
L _y	length of the computational domain in the Y direction	X, Y	dimensionless space coordinates
Nu	Nusselt Number	X _{r1}	reattachment length of adjacent vortex
PV	Primary Vortex	X _{r2}	reattachment length of primary vortex
Re	Reynolds Number	X _d	detachment length for secondary vortex
SV	secondary Vortex	ρ	density of air
u, v	velocity components in m/s	μ	dynamic viscosity

1. INTRODUCTION

Impinging jets are widely used in industries, because of their high heat removal rates. They are utilized for cooling of electronic equipment, particularly in chip arrays, due to their large heat dissipation. They are also used in turbine blade cooling, coating and tempering of glass and metal, engines, and Short Take-Off and Vertical Landing

(STOVL), due to their high heat and mass transfer rates, and high efficiency. Previous researchers have dealt jet impingement related to a turbulent regime, because of industrial applications. But in the cooling of microelectronic equipment, due to limited space, size and power input, a high velocity airstream for the cooling the same is not required because the equipment which occupies small space needs intense cooling. A low jet exit Reynolds

number is needed, to avoid high pressure in the jet impingement region. Therefore, only the laminar regime alone is preferred for the present investigation.

Jambunathan AR. *et al.* (1992) have summarized a comprehensive review of the heat transfer correlation for the single circular jet impingement. They have reported the heat transfer rate for different nozzle geometries, the Reynolds number, and the distance between the jet and the impingement plate. Sivasamy *et al.* (2007) have numerically studied the dynamics of the vertical slot single impinging jet on to a wall for the laminar flow regime. They have presented a detailed study of the horizontal velocity profile, the reattachment length, and the detachment length. A numerical study on a 2D laminar incompressible slot jet has been carried out by Sivasamy *et al.* (2008). They have concluded that Nu increases with the increase of the Reynolds number and the Prandtl number. Arquis *et al.* (2006) summarized a report on the cooling of an array of multiple protruding resources by a single laminar slot air jet. They concluded that the surface Nusselt number attained its maximum value at the block under the air jet impingement. Promvongse *et al.* (2010) have numerically analyzed the heat transfer rate for 45° inclined baffles for a square channel. They have found out that the 45° baffles generate more induced vortex flow throughout the channel, leading to an enhanced heat transfer rate. Bula *et al.* (2000) have performed a numerical investigation on the conjugate heat transfer performance of a single slot jet. They have concluded that the heat transfer performance is affected more by the Reynolds number, compared to the plate thickness and its thermal conductivity. Ertan Baydar *et al.* (1999) experimentally conducted a confined air jet impingement for a low Reynolds number in the range of 300-10,000. They concluded that the presence of the peak Nusselt number depended on the sub atmospheric region. Kazuyoshi *et al.* (2001) experimentally examined the heat transfer rate for twin inclined jets. They observed that the primary peak Nusselt number would occur in the stagnation region and the secondary peak Nu would occur at a downstream location. Buddhika (2009) has found out that the separation distance, frequency and the Reynolds number are the factors affecting the oscillatory jet impingement. Tesar and Barker (2002) studied the effect of the Reynolds number on the impinging jet flows. They reported that four regimes were identified with different flow characters on increasing the Reynolds number. They have added that even for a low Reynolds number laminar flow, the dominant vortices were identified in the flow regime. Sahoo and Sharif (2004) conducted a numerical investigation on the slot jet impingement cooling of a constant heat surface confined by a parallel wall. They reported that the average Nusselt number at the heated surface would not significantly change with respect to the Richardson number, for a particular aspect ratio and Reynolds number. Sparrow and Wong (1975) employed the naphthalene sublimation technique to analyze the heat transfer coefficients, due to an impinging slot-

jet in the laminar region. It was concluded that the increase in the aspect ratio would reduce the heat transfer rate and an increase in the Reynolds number would increase the heat transfer rate. Jafara *et al.* (2012) obtained the fluid flow field characteristics for the liquid jet impingement for various Reynolds numbers. They reported that the inertia force of the fluid, width of the jet, the distance between the jet and plate were more influencing parameters compared to the surface roughness and stagnation region. Dee Hee Lee *et al.* (2011) has experimentally conducted an investigation on the laminar impingement unsteady slot jets on a surface. They concluded that for the same jet-to-plate distance, Nu increased with an increase of Re, and for the same Re, Nu decreased with an increase of the jet to plate distance. Liu Haiyong (2011) has conducted experimentally measured the flow field parameters in a trapezoidal duct by using an induced swirl jet. He has indicated that small jets impinge the target wall effectively, while large jets are accompanied by a counter clockwise vortex on the upper field. Aldabbagh *et al.* (2002) applied the finite volume method, to find out the flow field and the heat transfer characteristics of impinging laminar multiple square jets. They concluded that the flow structures of the multiple jets were affected by the distance between the jet and the plate. Peng Wang *et al.* (2014) carried out numerical investigations on the flow and heat transfer behaviors of turbulent jet impingement. According to their numerical investigation, the SST k- ω method is a more appropriate model for the calculation of the heat transfer characteristics. Armaly *et al.* (1983) found out the reattachment lengths for a wide range of Reynolds numbers. They have reported that with the increase of the Reynolds number, the vortex size and reattachment length also increase. Forced convective heat transfer by a plane jet on a flat plate was addressed by Kanna *et al.* (2005). They have highlighted the fact that the local Nusselt number increases with the increase of the Reynolds number, and also the peak Nusselt number moves in a downstream direction. Kanna *et al.* (2006) conducted a detailed study on the reattachment length for the backward facing step. They summarized the different reattachment lengths for various Reynolds numbers. David *et al.* (2012) carried out numerical investigations on the heat transfer characteristics of two dimensional sudden expansion flow, using a nano fluid. They noted that the recirculation eddy was a much greater enhancing factor of heat transfer in the inlet region.

Buchlin (2011) compared the experimental investigation and numerical simulation in convective heat transfer especially in the impinging gas jet arrangement. He proposed the design correlation for different parameters.

The present authors (Muthukannan *et al.* 2014) conducted a numerical study only on the fluid flow characteristics, of a laminar slot jet on a solid block mounted on a horizontal surface. In their previous research work they found the flow field characteristics for Re ranging from 50 to 300, block

height, ranging from 0.25 to 1.0, and block width, ranging from 0.25 to 1.75 as the baseline case of AR5. The previous work has been confined by changing the AR ranging from 2 to 5 as the baseline case of Re 150.

From the open literature, it is confirmed that so far, most of the studies are concerned with the heat transfer analysis by varying the parameters like high Re and AR only on a flat plate. But in the case of microelectronic equipment, the area that needs to be cooled is a small one (Chiriac *et al.* (2002) as well as a laminar regime. Researchers have identified that vortex formation enhances the heat transfer rate, and at the reattachment point or nearer to the reattachment point the heat transfer rate attains its peak value. The size of vortex is an important parameter, as it directly affects the transport phenomena very effectively. It is an area of local as well as global fluid transport. The induction of so many vortices in a flow would render the flow turbulent. So, it is a measure that how fast a flow is going to be fully developed. Also it induces the heat as well as momentum transport over the region where it is formed. The heated walls in the vortex region get cooled since the cool fluid is drawn into the vortex region due to less pressure inside it so the larger the vortex more is the transport phenomena both in momentum and heat transfer conditions until and unless the flow is laminar. So, the present paper is focused to find out the heat transfer characteristics as well as the flow field characteristics. The primary aim of the study is to investigate the flow field and heat transfer characteristics on a solid block, and in downstream locations during jet impingement by modifying aspect ratio and the Reynolds number.

2. PROBLEM DESCRIPTION

The schematic diagram of the single slot jet impingement on a solid block is shown in figure 1(a). The jet emanates from a nozzle of normalized width W , with a uniform velocity u , impinges on a block, and reattaches on a bottom wall, which is called the hot wall located at a distance of L_y from the nozzle. The velocity in the X direction is regarded as ‘ u ’, and in Y as ‘ v ’. U (u/D_h) and V (v/D_h) are normalized by the horizontal and the vertical velocity components and are divided by the hydraulic diameter (D_h). The computational domain is symmetric about the vertical or y -axis. In order to save the computing time and power, only half of the domain is regarded for the problem configuration (Sivasamy *et al.* (2007)). The jet exit velocity (u) is encoded by using the formula: $Re = (\rho U D_h / \mu)$ where ρ denotes the density of the fluid; D_h is the hydraulic diameter, and μ is the dynamic viscosity of the fluid.

2.1 Numerical Procedure

Assumptions

In the present investigation, the following assumptions are made:

- The physical properties of the air are assumed

to be constant.

- The no slip condition has been applied to the hot and cold walls.
- The flow is assumed to be two dimensional, incompressible and laminar.
- Non-conjugate heat transfer alone is analyzed; i.e., the thickness of the bottom slab of the bottom wall in heat transfer is neglected, and the block surface as well as the impinging plate as a whole is assumed to be maintained at a constant temperature that is higher than that of the inlet jet and upper confinement plate.
- The influence of the body force is negligible.
- The normalized jet width is considered as 0.5 for the present investigation in order to consider the hydraulic diameter (D_h) as unity.

2.2 Governing Equations

Fig 1(a) shows the computational domain of the problem and the Cartesian co-ordinate system is followed in the present study. Since the computational domain is assumed to be two dimensional, the whole computational domain can be described as the following set of differential equations in non dimensional form (Sivasamy *et al.* 2007, 2008);

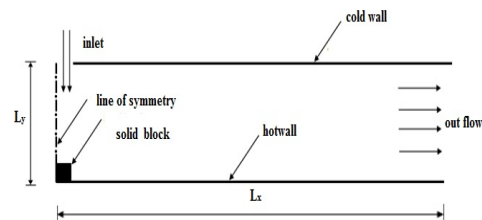


Fig. 1 (a). Schematic diagram of the physical model and the coordinate system

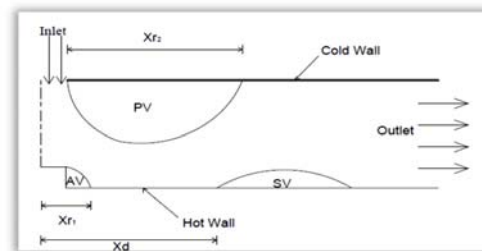


Fig. 1 (b). Definition of the Reattachment and Detachment lengths

Continuity equation:

$$\frac{\partial U}{\partial X} + \frac{\partial V}{\partial Y} = 0$$

X-momentum equation:

$$U \left(\frac{\partial U}{\partial X} \right) + V \frac{\partial U}{\partial Y} = - \frac{\partial P}{\partial X} + \frac{1}{Re} \left(\frac{\partial^2 U}{\partial X^2} + \frac{\partial^2 U}{\partial Y^2} \right)$$

Y-momentum equation:

$$U \frac{\partial V}{\partial X} + V \frac{\partial V}{\partial Y} = - \frac{\partial P}{\partial Y} + \frac{1}{Re} \left(\frac{\partial^2 V}{\partial X^2} + \frac{\partial^2 V}{\partial Y^2} \right)$$

Energy equation:

$$U \frac{\partial \theta}{\partial X} + V \frac{\partial \theta}{\partial Y} = \frac{1}{\text{RePr}} \left(\frac{\partial^2 \theta}{\partial X^2} + \frac{\partial^2 \theta}{\partial Y^2} \right)$$

The non-dimensional variables considered for this problem are,

$$X = Lx / D_h, Y = Ly / D_h, U = u / U_{in}, V = v / U_{in} \quad P = p / \rho U_{in}^2$$

$$\text{Re} = (\rho U_{in} D_h / \mu) \text{ and } \text{Nu} = \left(-\frac{\partial \theta}{\partial Y} \right)_{y=0}$$

where $\theta_f = \frac{T_f - T_c}{T_h - T_c}$ is the non dimensional temperature in the fluid region and

$\theta_s = \frac{T_w - T_c}{T_h - T_c}$ is the non dimensional temperature in the solid region.

The term θ_s is always 1 for the non-conjugate case, i.e., the effect of the slab thickness is neglected. Here, the temperature of the wall is assumed as the temperature of the hot fluid ($T_w = T_h$).

3. NUMERICAL APPROACH AND PROCEDURES

The steady state, two-dimensional Navier – Stokes, and energy equations for the incompressible flows in the Cartesian coordinates, are used for the present investigation. The steady state numerical investigation is done to capture the fluid flow and heat transfer characteristics on a single solid block, under a single confined slot jet by using the Computational Fluid Dynamics (CFD) techniques. The commercial package gambit 2.4 (preprocessor) is used to model the domain, with the maximum nodes of 3.4×10^5 . The air is engaged as the working fluid. The boundary conditions employed are, constant uniform velocity in order to satisfy the overall continuity requirement and temperature of the jet inlet, no slip condition at the bottom wall and top wall $u = v = 0$, symmetry condition at $L_x = 0$, fully developed flow at the channel exit ($\frac{\partial u}{\partial x} = \frac{\partial v}{\partial x} = 0$), and constant wall temperature at the top and bottom walls. The grid employed in this simulation is fine near the impingement surface and coarse at other regions, where the flow parameters have high gradient. The mesh gets coarser gradually along the downstream of the computational domain, in order to obtain an accurate result. A non-uniform structured quadrilateral element is used to discretize the entire computational domain, which does not contain any curved surfaces or sharp edges.

Fluent 12.0 (processor) is used to analyze the fluid flow for various situations. The pressure based solver is used, as the fluid is incompressible. SIMPLE (Patankar 1980) (Semi-Implicit Method for Pressure Linked Equation) is applied with the discretization technique, as the Green-Gauss Cell based, with both the pressure and momentum equations being solved, to the accuracy of the second order. The convergence criteria of the scaled residual for continuity, X velocity, Y velocity and energy, are set to 10^{-5} .

The Tecplot 9.0 (postprocessor) is used to construe the result for obtaining the contour plots of X velocity, Y velocity and streamline contour.

3.1. Validation of the Code

With a view of confirming the present algorithm, the present code has been tested against that of Sivasamy *et al.* Because of lack of experimental data for the present situation, the validation is done against Sivasamy *et al.* (2007, 2008) whose geometry and flow parameters are quite similar, with the exception of the solid block.

For validation, the coefficient of friction and Nusselt number are extracted at the bottom wall using the present algorithm, and compared with the work of Sivasamy *et al.* (2007, 2008). Figures 2 and 3 show good agreements with Sivasamy *et al.* (2007&2008) and indicate that this algorithm is suitable to be applied for the present investigation.

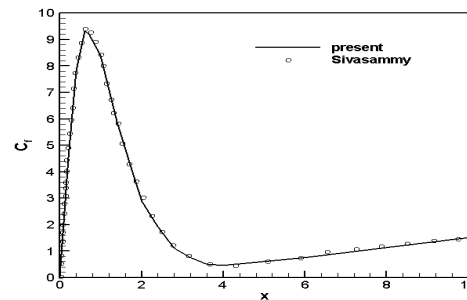


Fig. 2. Validation of C_f against Sivasamy *et al.* (2007).

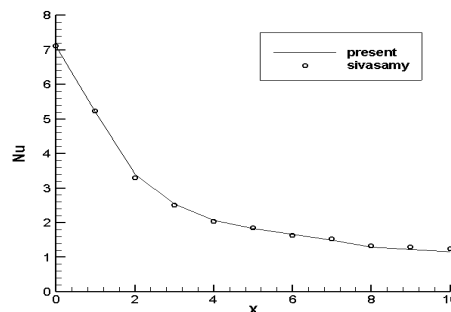


Fig. 3. Validation of the bottom wall Nusselt number against Sivasamy *et al.* (2008).

3.2 Grid Independence Study

From the previous works (Sivasamy *et al.* (2007, 2008), it is proved that the length of the domain in the X (L_x/D_h) direction has been chosen as $20 D_h$ to attain a fully developed condition, i.e., ($\frac{\partial u}{\partial x} = 0$) at the exit. Depending upon the aspect ratio, the scaling in the normal direction is chosen. A series of grid refinement studies is done for $AR=5$ and $Re=300$ in order to give an intense impression upon the complexity in the problem. The average Nu has been taken in the bottom wall for checking the grid independence study (Table 1). Table 1 discloses that the prediction of Nu does not substantially

change grid No 4. The variation of Nu between grid no 4 and grid no 6 is 1%. So, grid No 4 is taken as the base line case for AR5 for all Reynolds numbers.

Table 1 Grid independence study

Grid refinement level	Total No of nodes	Average Nu Number for the bottom wall
Grid 1	259246	2.7700
Grid 2	274584	3.4567
Grid 3	289584	3.7890
Grid 4	304584	4.1028
Grid 5	319922	4.1256
Grid 6	335260	4.1364

4. FLOW FIELD INVESTIGATION

4.1. Effect of Re on Flow Field for AR=2

In this case, the Reynolds number is considered as the variable parameter. The Reynolds number is varied from 50 to 300 with the step of 50. The jet width (W) is taken as 0.5 for all cases, in order to have a hydraulic diameter as the unity ($D_h=1$), taking the line of symmetry into account. The block height and the block width are considered, as constant and equal to 0.5. Four different values of $L_y = 1, 1.5, 2$ and 2.5 are considered which provide AR (L_y/W) as 2, 3, 4 and 5 respectively. In the present case, the Aspect Ratio (AR) is equal to 2, which indicates that the length of the domain in the Y direction is equal to 1. The length of the domain in the X direction is taken as 20 to achieve a fully developed condition at the exit.

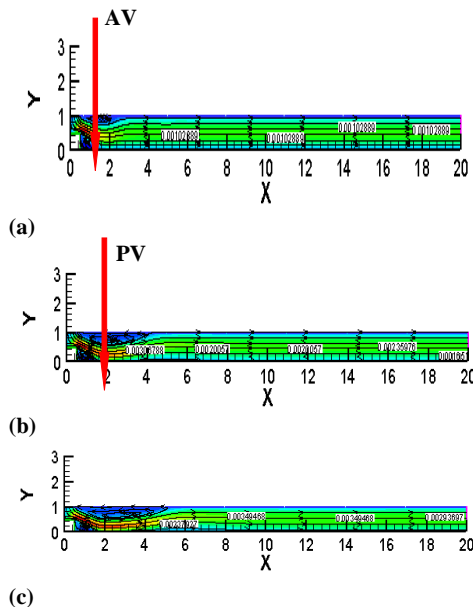


Fig. 4. Effect of Re on flow field (AR=2, W=0.5, w/Dh=0.5, h/Dh=0.5) (a) Re=100, (b) Re=200, (c) Re=300.

Figure 4(a-c) shows the effect of changing the Reynolds number during the investigation of the flow field in the channel with AR=2. From Figure 4(a-c),

it is inferred, that the jet impinges on a block, and makes a turn on the right side of the computational domain. After the impingement on the block, the flow reattaches on the lower wall. Due to the sharp turn, a flow separation occurs in the lower wall, called the adjacent vortex (AV), which is denoted in Figure 4(a). While increasing the Reynolds number, there is a formation of vortex which is at the top of the wall, called the primary vortex (PV) (which is denoted in Figure 4(b)) due to the entrainment of air (Sivasamy *et al.* (2007)). The size of the vortices intensifies with the increase of the Reynolds number (Sivasamy *et al.* (2007 and 2008)). The adjacent vortex center and primary vortex center also shift correspondingly in downstream, with the increase of the Reynolds number (Sivasamy *et al.* (2007&2008)). The stream lines which are parallel to each other justify the assumption, that the flow is fully developed at the exit (Kanna *et al.* (2006)). For the sake of simplicity, the streamlines for $Re = 100, Re=200$ and $Re=300$ are given in all cases of AR.

4.1.1. Horizontal Velocity Profile from Various Downstream locations

From figure 5(a-d), it is confirmed that the horizontal velocity attains a peak value at the location of $X=1$. The protrusion of the negative velocity at $X=1$ indicates the formation of the adjacent vortex nearer to the solid block. The peak velocities at $X=1$ are $8.399 \times 10^{-4}, 2.031 \times 10^{-3}, 4.537 \times 10^{-3}$ and 7.11×10^{-3} for $Re=50, 100, 200$ and 300 respectively. Then, due to the expansion of the wall jet (Kanna *et al.* (2005)) in the downstream direction, the velocity reduces to 0.0005299, 0.001098, 0.002160 and 0.003240 respectively at the exit ((Sivasamy *et al.* (2007 and 2008)). The magnitude of velocity extends in the negative direction at $X=1$, which signifies the growth of the adjacent vortex with the increase in the Reynolds number. Even for the $Re=300$, there is no fluctuation in the fluid path and further Cdownstream of $X=10$. The parabolic horizontal velocity profile for all Re's reflects that the flow is in a fully developed condition at the exit. From Figure 5(a-d), it is concluded, that with the increase of the Reynolds number, the peak horizontal velocity also increases and moves downwards.

4.2. Effect of Reynolds Number on flow Field for AR=3.

In the present work, the AR is equal to 3 which indicate that the length of the domain in the Y direction is considered as 1.5.

Figure 6(a-d) shows the effect of the Reynolds number on the investigation of the flow field with respect to AR=3. From the figure 6(c), it is observed that for AR=3, when the Reynolds number increases from 150 to 200 (shown in figure 6(c)) the flow separation occurs at the hot wall due to the formation of a new vortex called the secondary vortex, which is due to the increased frictional force and holding the effect of the primary vortex (Sivasamy *et al.* (2007)). From the figure 6 it is concluded that with the increase of the Reynolds number, the secondary vortex size is also intensified.

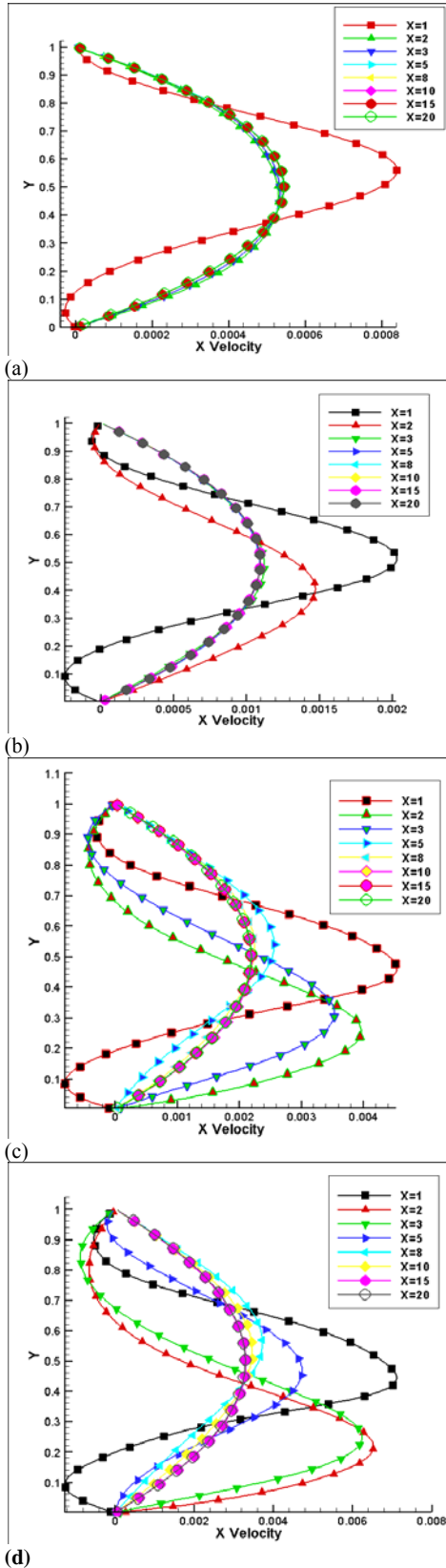


Fig. 5. Horizontal velocity plot of AR 2 for different Reynolds Numbers: (a) Re=50; (b) Re=100; (c) Re=200 ;(d) Re=300.

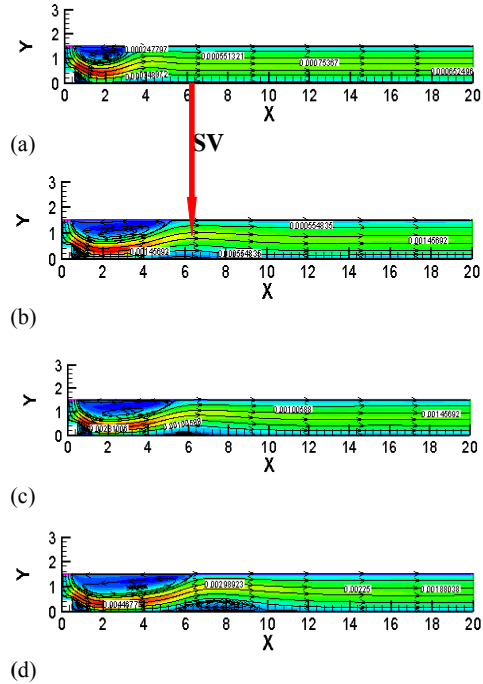


Fig. 6. Effect of Re on the flow field (AR=3, W=0.5, w/D_h=0.5, h/D_h=0.5) (a) Re=100, (b) Re=200, (c) Re=250, (d) Re=300.

4.2.1. Horizontal Velocity Profile from Various Downstream Locations for AR=3

From figure 7(a), it is evident that the horizontal velocity attains its peak value at the location of X=1 for the Reynolds number of 50. There is no impact of the primary vortex on the flow field because of the absence of negative velocity profile for Re=50. With the increase of Re from 100 to 200, the position of peak velocity is also shifted from X=1 to X=2. Due to the increased size of the primary vortex, the negative velocity profile is achieved for X=1, X=2 and X=3 (Figure 7(b)). For the Reynolds numbers 200 and 300 (figure 7(c) & 7(d)), the flow attains a fully developed condition only at X=15

4.3. Effect of Re on the Flow Field for AR=4.

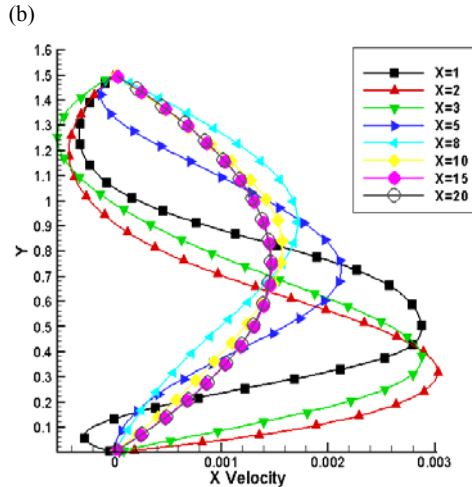
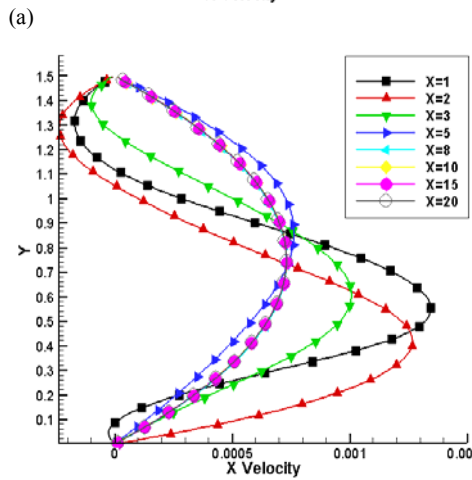
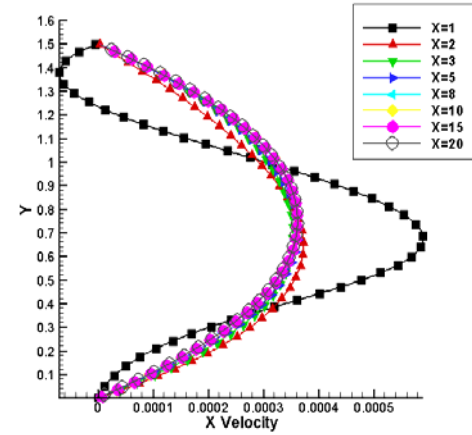
In the present investigation, the length of the domain is equal to 2, in order to attain the aspect ratio (L_y/D_h) of 4.

Figure 8 shows the influence of the Reynolds number on the flow field for AR=4. The top wall is bounded with the primary vortex, and the bottom wall is bounded with the adjacent vortex and primary vortex. As the Reynolds number increases, the primary recirculation eddy grows larger, and pushes the secondary recirculation eddy to the downstream direction (sivasamy *et al.* (2007)).

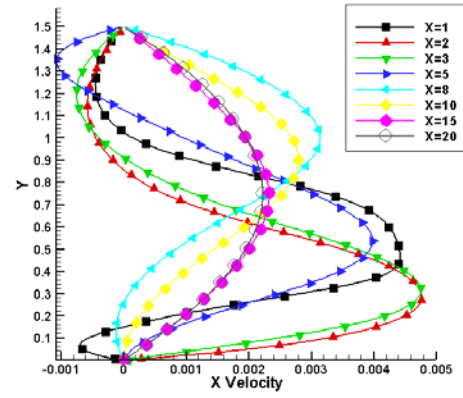
4.3.1. Horizontal Velocity Profile from Various Downstream Locations for AR=4

From the figure 9, it is inferred, that for Re=50 at

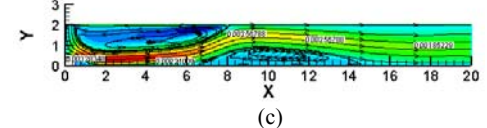
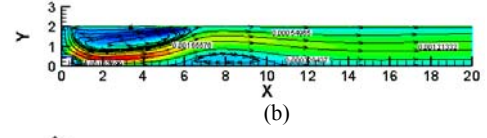
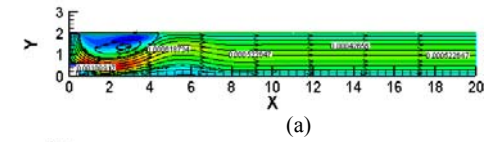
X=5 itself, the flow becomes a developed one. The negative velocity at X=1 indicates the formation of a primary vortex. The increase in the negative protrusion indicates the growth of the primary vortex. When Re increases, the length at which the flow becomes fully developed and is also increasing in the downstream direction. The parabolic profile for all Re's represents the flow in a fully developed condition at the exit.



(c)



(d) Fig. 7. Horizontal velocity plot of AR 3 for different Reynolds Numbers: (a) Re=50; (b) Re=100; (c) Re=200 ;(d) Re=300.



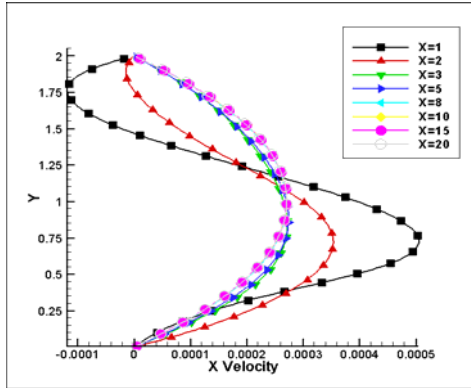
(c) Fig. 8. Effect of Re on the flow field (AR=4, W=0.5, w/Dh=0.5, h/Dh=0.5) (a) Re=100, (b) Re=200, (c) Re=300.

4.4. Effect of the Reynolds Number on the Reattachment Length (X_{r1}) and Detachment Length (X_{r2})

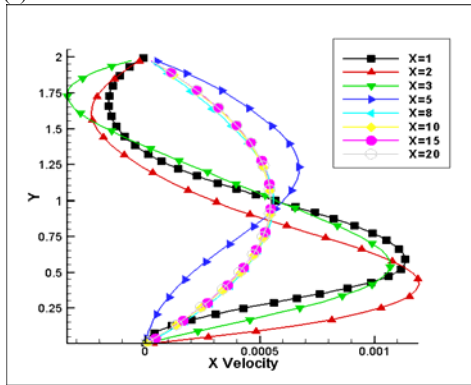
From the open literature, it is observed that the reattachment length, X_{r1} , is the horizontal distance between the stagnation point and the attachment point after the block, and the distance between the stagnation point and the point at which the flow detaches from the impingement plate is the detachment length, X_d . The horizontal distance due to entrainment of fluid which would reattach on top wall is called reattachment length (X_{r2}) of primary vortex.

The reattachment and detachment lengths are observed, by identifying the direction change in the bottom wall velocity. Obviously, the bottom wall velocity changes in the direction, due to the vanishing of the shear stress. Figures 10 (a) and 10 (b) show the findings of the reattachment lengths (X_{r1} & X_{r2}) and detachment length (X_{r2}) with respect to the Reynolds number (Re). The reattachment lengths and detachment length are the direct function of the Reynolds number (Sivasamy *et al.* (2007 and 2008)). The reattachment length

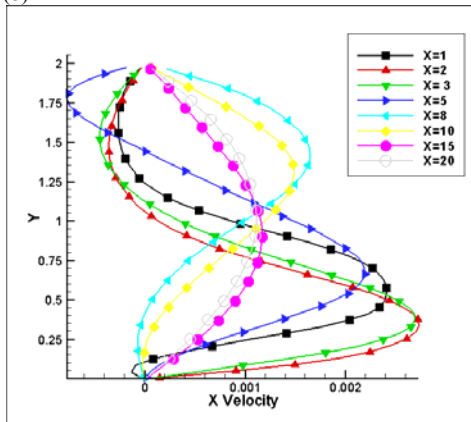
shows the non linear increasing trend for all AR's. But in the case of the detachment length for AR=3, there is a trivial change with respect to the Reynolds number. It denotes that the secondary vortex does not move significantly in the X direction. For AR4 and AR5, there is a 25% and 53% increment, in the detachment length which shows that there is a marginal increase in the separation of the flow. The effect of the Reynolds number on the vortex centers in the Y direction with respect to the AR is not plotted. Because, there is a negligible movement of the vortex center in the Y direction, compared to the X direction.



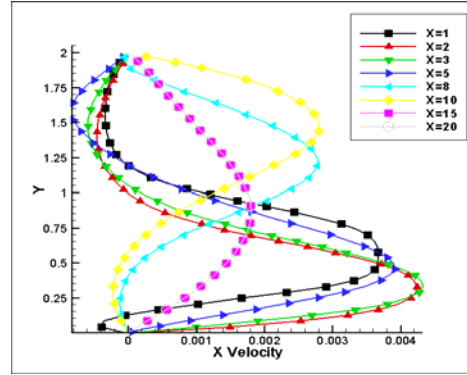
(a)



(b)



(c)



(d)

Fig. 9. Horizontal velocity plot of AR 4 for different Reynolds Numbers: (a) Re=50; (b) Re=100; (c) Re=200; (d) Re=300.

$$X_{r1} = \left(\frac{1.2222}{AR} \right) + (0.2000 * \log(Re) - 0.2072)$$

$$X_{r2} = \left(\frac{3.1802}{\log(Re)} \right) - \left(\frac{11.9424}{AR} \right) - 6.9657$$

The above correlation is recommended to find out the reattachment lengths (X_{r1} , X_{r2}) for the different AR's and Re's. The comparison between the simulation and the results is plotted in Fig 10 (d). From the figure 10(d) it is observed, that the suggested correlation is the best fit for a high Re. The correlation is not found for the detachment length, due to the non-availability of required data.

4.5. Effect of the Reynolds Number on the Vortex Center

Figures 11(a), 11(b) and 11(c) summarize the location of the vortex center for different Reynolds numbers. It is observed that with the increase of the Reynolds number, the centers of the vortexes move in a downstream direction (Sivasamy *et al.* (2007 and 2008)). In the case of the adjacent vortex centers of AR4 and AR5, they are show a similar trend with a small increment. From the figure 11(d), the exit velocities is calculated and are found to be 0.001081, 0.0007273, 0.00054 and 0.000437 for AR2, AR3, AR4 and AR5 respectively. It is interesting to note that there is a small fall in the velocity at the exit, when the AR increases from 4 to 5. It reflects the small increment of the shifting in the adjacent and primary vortexes in the downstream direction. Hence, it is concluded that with further increase of AR5, there is no marginal change in the adjacent vortex center, with respect to the Reynolds number. In the case of secondary vortex center, there is a noteworthy movement in vortex center when AR increases. For AR=5, the secondary vortex center in X coordinate increases gradually and constantly. On the other hand the vortex center in Y coordinate first increases rapidly but as the velocity increases the static pressure at the region outside the secondary vortex and it is this pressure that limits the increase of center of Y as the Reynolds number is increased [not shown in graph].

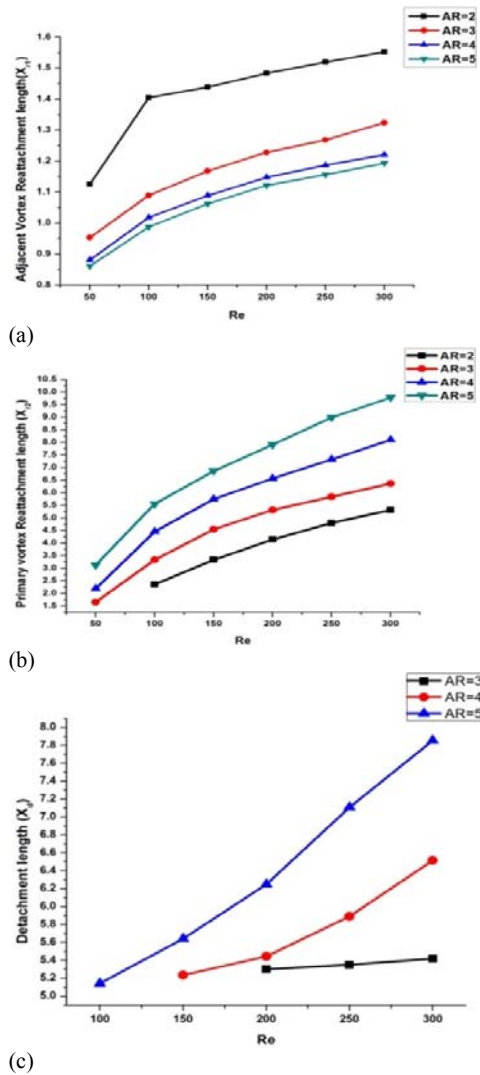


Fig. 10(a), 10(b) and 10(c) Effect of Re on the reattachment lengths (X_{r1} , X_{r2}) and detachment length (X_d) for different AR's.

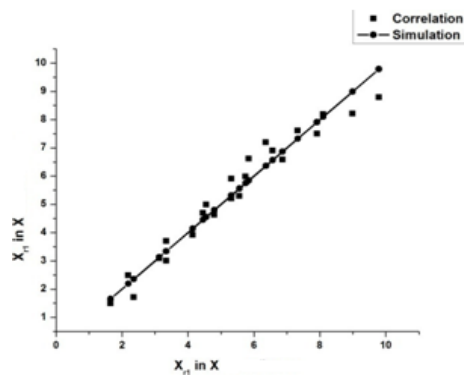


Fig. 10(d). Comparison between the correlation results and simulation results.

The center of the primary vortex in X coordinate is not predicted in case of AR5, for the Re=250&300, due to the formation of the pairing of the vortex problem.

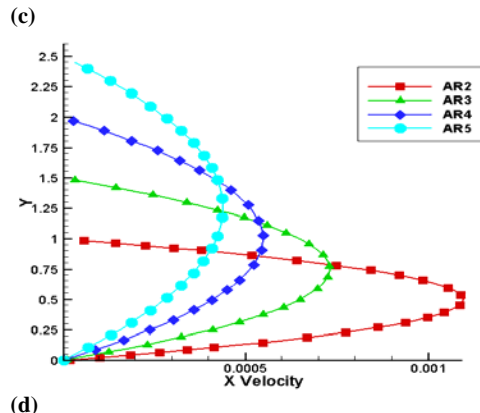
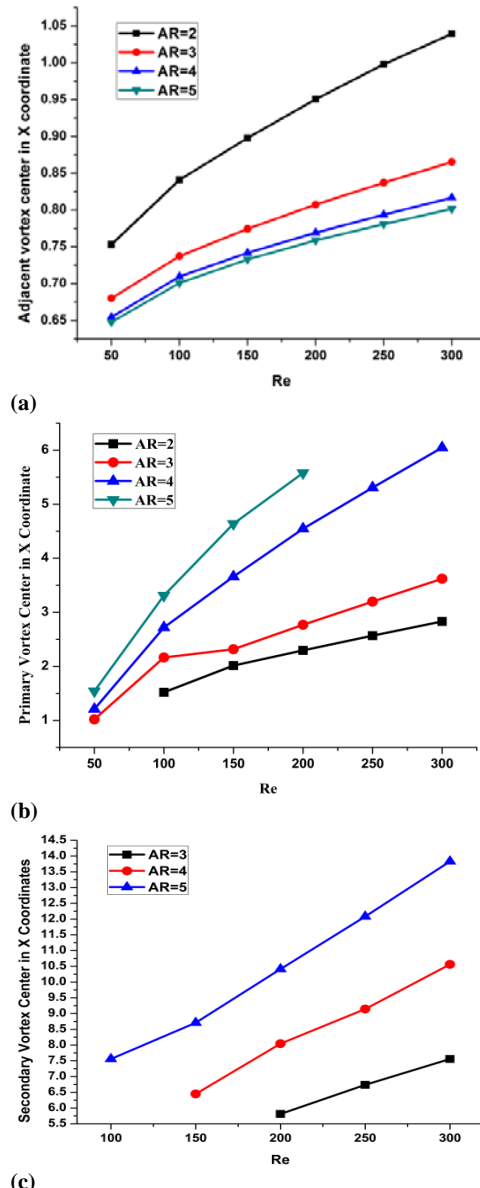


Fig. 11(a), 11(b) and 11(c). Effect of Re on Adjacent, Primary and Secondary vortex centers in the X coordinate for different ARs.(d) Effect of Re=100 on the exit for different ARs.

5. INVESTIGATION OF HEAT TRANSFER

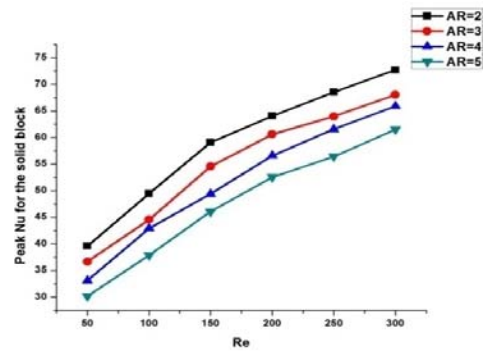
In general, the heat transfer rate is anchored on the jet strength, which is defined by the inertia force. Because of the fact that the physical properties of the fluid are kept constant, the present numerical investigation is confined to change the Reynolds number, and the distance between the jet and the block. In the present numerical investigation, the jet impinges on the top face of the block, (i.e., the impingement surface or the stagnation surface), and then, turns onto the right-hand side of the computational domain. The average Nusselt number and peak Nusselt number calculations for the entire computational domain are divided into two segments.

1. Impingement region (top face of the block)
2. Other surfaces (combination of recirculation region and wall jet region)

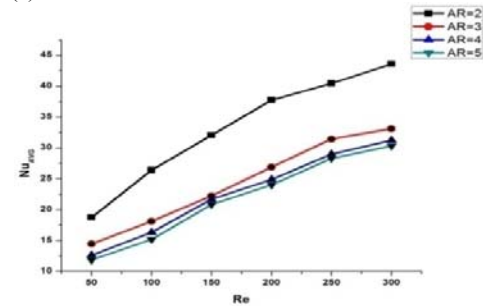
As expected, the average Nusselt number for the impingement surface is high, and the average Nusselt number also intensifies with the increase of the Reynolds number. The local Nusselt number distribution along the bottom wall is also reported in the present investigation.

5.1. Effect of the Reynolds Number on the Impinging Surface

The average Nusselt number and peak Nusselt number for the solid block surface are shown in Figs 12(a) and (b). It is concluded that the apex of the Nusselt number is evaluated at the impinging surface, irrespective of the Reynolds number and aspect ratios, at the extreme right end of the edge, due to the sharp edge of the solid block (Fig.17). It is observed that the Nusselt number depends largely on the Reynolds number, compared to AR. When the AR increases, the distance between the jet and block also intensifies, resulting in decreased momentum of the jet, which impinges on the block. The decreased momentum effect (inertia force) will diminish the heat transfer in a significant manner (sparrow *et al.* (1975)). From Fig. 12, it is clear that when the aspect ratio increases from 4 to 5, there is a small fall (maximum of 7% only in the Reynolds number 100) in the heat transfer rate. So, it is concluded, that further increase of the aspect ratio of 4 will not significantly affect the heat transfer rate in the solid block. For the Reynolds number of 50, when the AR is increased from 2 to 5, there is a high fall (42%) in the heat transfer rate, and for the Reynolds number of 300, there is a low decrease in heat transfer rate (30%). From the figure 12, it is noticed that for the same AR, there is a steep increase in heat transfer rate up to the Reynolds number of 200, and then, there is a marginal drop in the increase of heat transfer rate. The following correlation is recommended to find out the peak Nusselt number in the solid block for an AR between 2 and 5, and the Re from 50 to 300. The maximum discrepancy between the correlation and simulation is 5% and the minimum is 0.8%.

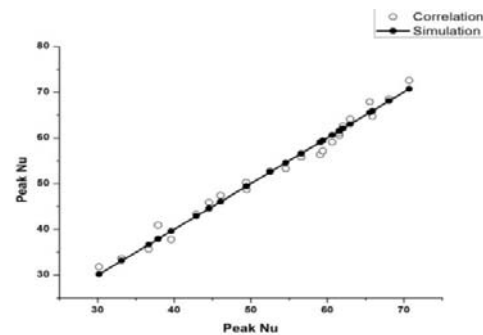


(a)

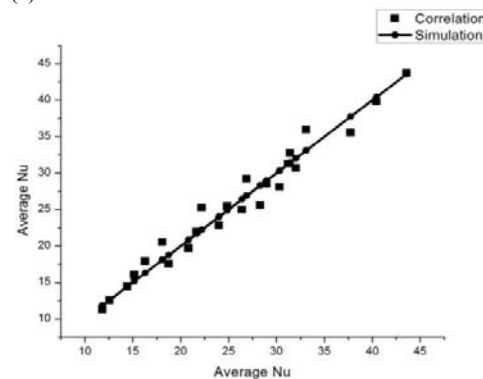


(b)

Fig. 12(a) and (b). Effect of Re on the Peak and Average Nu on the solid block surface.



(a)



(b)

Fig. 13(a) and 13(b). Goodness of Correlation and simulation results for the peak Nu and Average Nu in the solid block.

$$\text{PeakNu}_{\text{forSolidblock}} = 10.1837 * 0.9441^{\text{AR}} * \text{Re}^{0.3644}$$

The following correlation is suggested to find out the average Nusselt number in the solid block for an AR between 2 and 5 and the Re from 50 to 300. The maximum discrepancy between correlation and simulation is 9% and the minimum is 0.1%.

$$\begin{aligned} \text{AverageNu}_{\text{forSolidblock}} &= 3.3339 * \text{AR}^{-0.4834} \\ &* \text{Re}^{0.5099} \end{aligned}$$

In Figs 13 (a) and (b), the correlation result along with computational result is compared for peak and average Nu for solid block.

Previously published experimental data state that the stagnation Nu depends on the square root of Re (lyte *et al.* (1994)). The suggested correlation for average Nusselt number depends on $\text{Re}^{0.5}$ and confirms the previous researcher's investigation.

5.2. Effect of the Reynolds Number on the Downstream location

In order to assess the heat transfer features associated in downstream direction i.e. apart from the block, Fig. 14 is plotted. From the Fig. 14, it is known that for the same Reynolds number, the average Nusselt number and peak Nusselt number decrease monotonically with respect to the AR. From Fig. 14, it is observed that at a downstream location for a low Reynolds number (Re 50 and Re 100), the peak Nusselt number's value has a small discrepancy, irrespective of the aspect ratios. Because at low Reynolds numbers in downstream locations, the size of the vortexes are smaller and the reattachment length is also the same. Furthermore, on increasing the Reynolds number to 100, the vortexes grow in size, which enhances the heat transfer to an appreciable percentage in the downstream locations. Close examination of the Average Nu (Fig. 14(b)) reveals that, for the Re of 50, when AR increases from 2 to 5, the minimum decrement (20%) is observed and for a Re of 300 a large discrepancy (28%) is observed (Samy *et al.* (1992)).

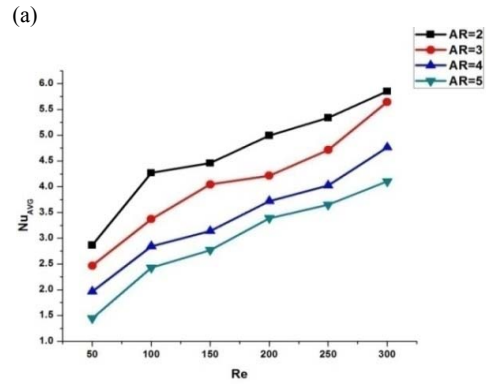
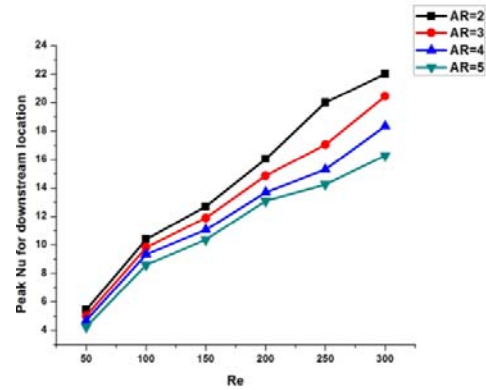
When the Re increases, the size of the primary vortex also increases, which leads to an increase in the length of the wall jet region. The thermal boundary layer thickness decreases in the wall jet region, with the increase of the inertia force which improves the heat transfer (Arquis *et al.* (2006)).

The following correlation is recommended to find out the peak Nusselt number in the downstream locations, for the AR between 2 and 5 and Re from 50 to 300. The maximum discrepancy between the correlation and simulation is 10% and the minimum is 3% for the Re of 300.

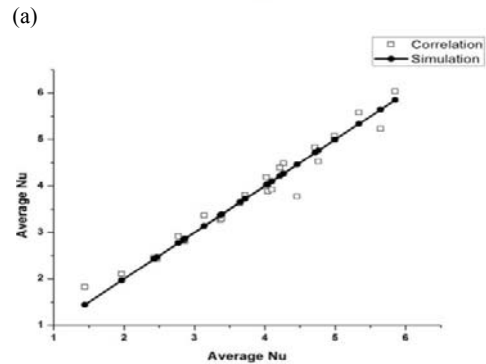
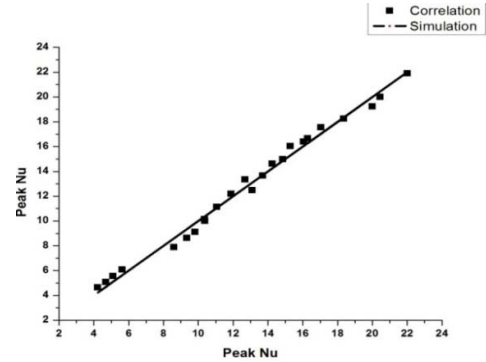
$$\begin{aligned} \text{PeakNu}_{\text{fordownstream}} &= 0.4463 * 0.9129^{\text{AR}} \\ &* \text{Re}^{0.7145} \end{aligned}$$

The following correlation is suggested to find out the average Nusselt number in the downstream location for the AR between 2 and 5 and for the Re from 50 to 300.

$$\begin{aligned} \text{AverageNu}_{\text{fordownstream}} &= 0.7006 * 0.8662^{\text{AR}} \\ &* \text{Re}^{0.4277} \end{aligned}$$



(b) Fig. 14(a) and (b). Effect of Re on the Peak and Average Nu on the downstream locations.



(b) Fig. 15(a) and 15(b). Comparison of the correlation results and simulation results for peak Nu and Average Nu in the solid block.

Figure 15(a) and (b) show the comparison of simulation result with correlation result. The figure 15 shows the good agreement between simulation and correlation results

5.3. Effect of the Reynolds Number on the Local Nusselt Number Distribution

Figure 16 shows the distribution of local Nusselt number for various Reynolds numbers and aspect ratios. The variation can be explained as, the impingement of cold fluid on to a block creates large differences in temperature. Hence, the Nu is larger and goes on increasing till the block width. As the block region is over the bottom wall is under the region of adjacent vortex. Since the vortex is a local transport phenomenon the local temperature difference between the wall and the fluid is less and hence the Nu number value decreases sharply. As one move along the x-direction, after the adjacent vortex region the Nu again rises slightly, then decreases and it becomes constant as the flow is fully developed.

In all the Fig. 16, the Nusselt number starts with a minimum value and reaches its peak value at the reattachment point or nearer to the reattachment point, due to the reduction in the thermal boundary layer thickness on the bottom wall of the computational domain. Beyond the peak value, the Nusselt number decreases in downstream direction, and reaches an asymptotic value due to the fact that the flow attains fully developed (David *et al.* (2012)). For the Reynolds number of 50 in the Nusselt number, there is no secondary peak formation due to low inertia force. The Nu number variation stabilizes or becomes constant even at X=4 in case of Re=50 since there is no formation of secondary vortex in this case. For the high Reynolds number a secondary peak in Nusselt number is noticeable in all plots of Fig. 16. Consequently, the separation of the flow accelerated due to the high inertia force. From the Fig. 16, it is noticed, that with the increase of the Reynolds number, the peak Nusselt number also moves in the downstream direction (Kanna *et al.* (2005), David *et al.* (2012)). The reason for this trend is that, the reattachment point, which holds the peak of the Nusselt number, increases with the increase of the Reynolds number. It can also be explained by proving that the evolution of recirculation is the reason for the shifting of peak Nu in the downstream direction (Kanna *et al.* (2006)). A rise in the Re results in shifting of asymptotic limit in downstream direction (David *et al.* (2012)). For the Re=300 and AR=5, large vortex gets broken into pairing of small vortices which decelerate the fluid flow (Hee *et al.* (2005)). As a result of this effect, bottom wall Nu falls to the abyss of Nu=0.52). This effect is clearly reflected in Fig. 16(d). From Fig. 16, it is seen that with the increase of Re, the apex of Nu also increases (Ishan *et al.* (2008)).

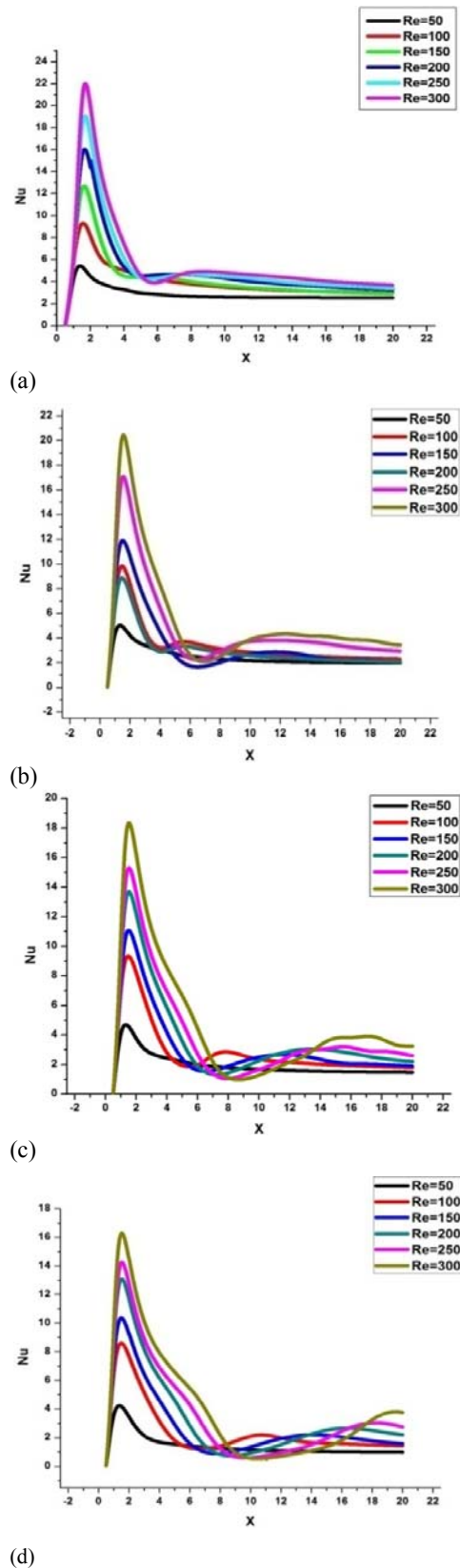


Fig. 16. Local Nu number distribution for different AR's. (a)AR=2, (b) AR=3, (c)AR=4, (d)AR=5.

6. EFFECT OF C_f

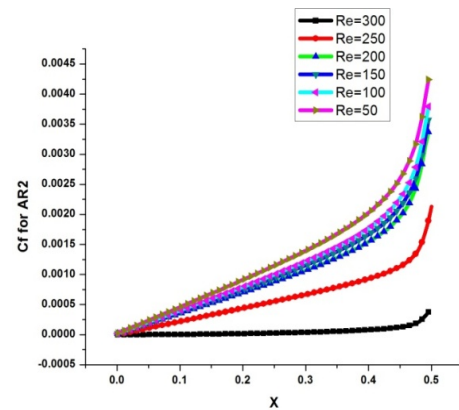
The coefficient of friction is also found out in the present investigation in order to find out the friction along the block and bottom wall.

6.1. Effect of C_f on Solid Block

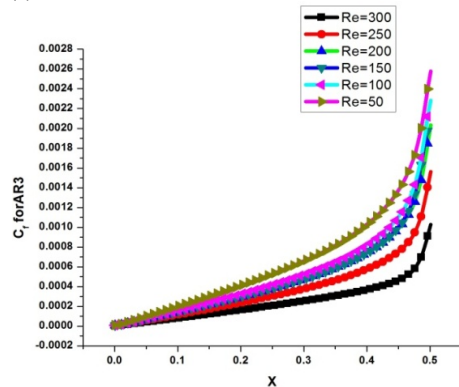
The skin friction is calculated along the solid block using the formula $C_f = \left(\frac{2}{Re}\right) \left(\frac{du}{dy}\right)$ (Ishan *et al.* (2008)). From the figure 17, it is inferred that the coefficient of friction decreases with the increase of Re (Hee *et al.* (2005)). The coefficient of friction attains the peak value at the extreme right end, due to the sharp edge of the block. From the figure 17, it is concluded that for every AR, Re=50 attains peak C_f compared to other Re's. This confirms that Re is the inverse function of C_f (David *et al.* (2012)). The subtle variation of C_f is observed with increasing Re and decreasing AR. From the graph, it is interesting to note, that the peak value of the coefficient of friction decreases with the increase of AR (Muthukannan *et al.* (2014)) (Fig. 18).

The following correlation is proposed to find out the peak value of C_f for various AR's. The Figure 19 shows the comparison between the simulation and correlation results.

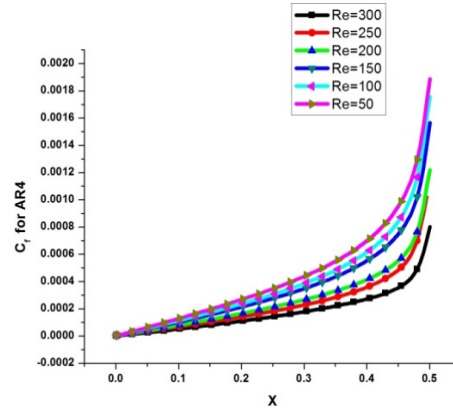
$$C_{f,Peak} \text{ for solid block} = 2.2031 * 10^{-2} + 4.2362 * 10^{-3} * AR - 1.8570 * 10^{-2} * AR^{0.5}$$



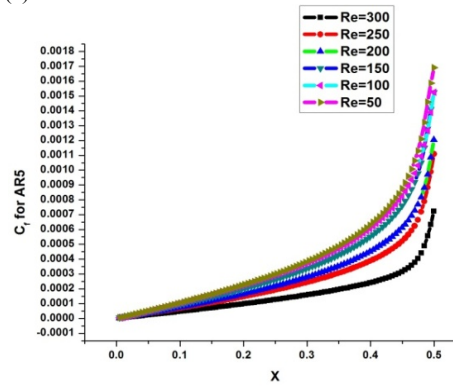
(a)



(b)



(c)



(d)

Fig. 17. Effect of C_f on the solid block for various aspect ratios (a) AR=2 (b) AR=3 (c) AR=4 and (d) AR=5.

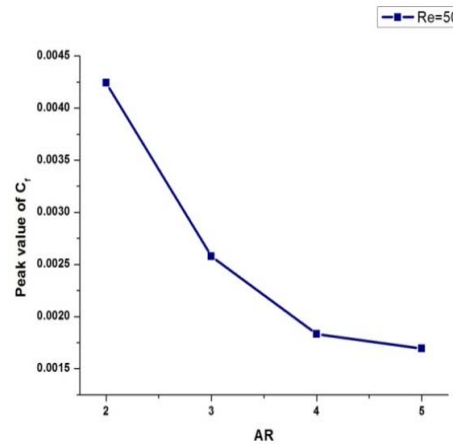


Fig. 18. Peak value of C_f in the solid block vs. AR.

6.2. Effect of C_f on Downstream Location

Figure 22 shows the variation of C_f along the bottom wall, with respect to AR for the constant Re of 300. The local skin friction coefficient drops due to the adjacent vortex nearer to the solid block and then sharply increases (primary peak) and again drops in the stream-wise direction. Due to the separation of flow (secondary vortex) that takes place in the downstream direction, there may be an

acceleration of the fluid. It induces an increase in friction again and a secondary peak in friction is formed. The C_f attains an asymptotic value which represents the flow in the fully developed condition (David *et al.* (2012)).

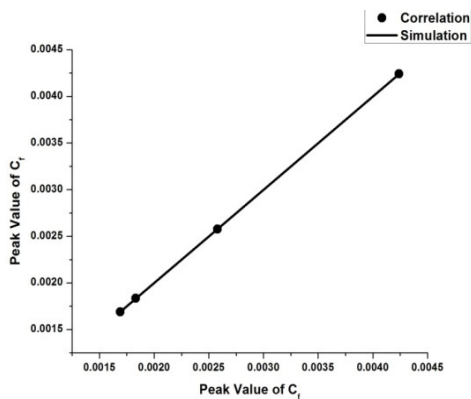


Fig. 19. Comparison of C_f between the correlation and simulation results.

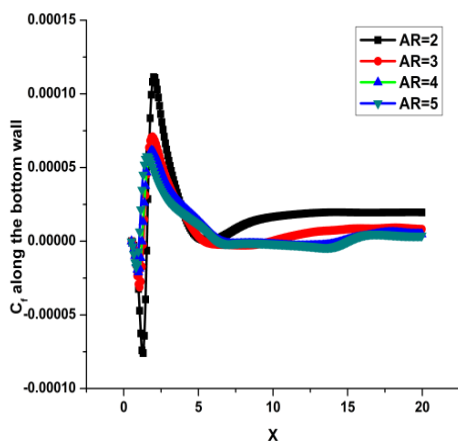


Fig. 20. C_f along the bottom wall for various AR's.

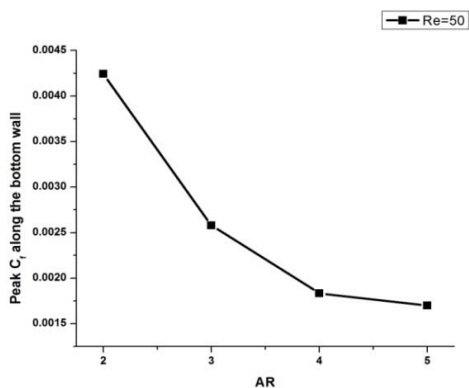


Fig. 21. Peak C_f vs Different AR's.

From the graph, it is revealed that the coefficient of friction decreases with the increase of AR. From figure 21, it is concluded that for a particular AR

the peak C_f is obtained for $Re=50$. The peak C_f decreases with the increase of AR (Sivasamy *et al.* (2007)).

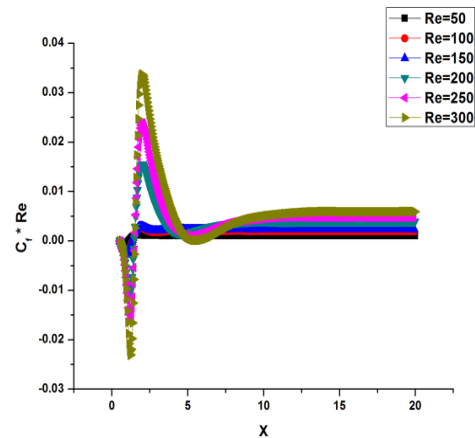


Fig. 22. C_f along the bottom wall for various Re for AR=2.

$$C_{f_{Peak}} \text{fordownstream} = 1.5339 * 10^{-2} + 2.1032 * 10^{-4} * AR^2 - 8.4481 * 10^{-3} * AR^{0.5}$$

Figure 22 shows the distribution of $C_f * Re$ for various Re's for a particular AR=2. The negative value of C_f denotes the recirculation eddy, and it intensifies with the increase of Re (Ishan *et al.* (2008)). For AR=2 there is no formation of secondary vortex leading to the vanishing of the secondary peak. This is revealed in fig 22. The constant value of C_f represents the flow in the fully developed condition.

7. CONCLUSION

In the present numerical investigation, the fluid flow along with heat transfer, while the jet impinges on a block, is investigated using commercial CFD codes. The computed flow fields and thermal fields in terms of the Aspect Ratio ranging from 2 to 5 with the Reynolds number ranging from 50 to 300 are analyzed in which the flow comes under the laminar regime.

The flow field parameters like reattachment length, detachment length, vortex centers and coefficient of friction are presented for various Reynolds numbers and aspect ratios. The average and peak Nusselt numbers are found for the solid block and downstream locations. The local Nusselt numbers along with the downstream location are also plotted for a wide range of Reynolds numbers and aspect ratios.

Due to the presence of the solid block, the hydrodynamic effect significantly creates the vortex nearer to the block, called the adjacent vortex. The size of the adjacent vortex intensifies with the increase of Re. There is no formation of a secondary vortex even for $Re=300$ for AR=2. But when the AR increases from 2 to 5 for the $Re=100$ itself, the secondary vortex is formed. From the

present investigation it is confirmed, that when AR increases step by step, the Re for the formation of a secondary vortex reduced drastically.

For the same Re, when AR increases, the length of the vortices also increases. For the same AR when Re increases, the vortex size also increases. The reattachment and detachment lengths increase, when the Re increases. For the same Reynolds number, the coefficient of friction decreases, when AR increases. The confinement surface or top wall and Re are playing key roles in vortex formation.

The average Nu and peak Nu shows a non linear increasing trend, when the Reynolds number increases, moreover a marginal depression occurs when AR increases. The Nu attains a peak value irrespective of Re and AR at the extreme right edge of the block, due to the sharpness of solid block. The local Nu reaches the peak value nearer to the reattachment point, and further in downstream locations reaches an asymptotic value which denotes that the flow has become a developed one. For the high Re, the secondary peak on Nu is observed in a downstream location.

The parametric investigation is helpful to predict the reattachment location, vortex center, peak Nu, average Nu and the coefficient of friction on the solid block, and in downstream location, while the jet impingement is on the solid block.

ACKNOWLEDGEMENTS

The constructive comments and suggestions of the reviewers are sincerely acknowledged by the authors.

REFERENCES

Aldabbagh, L. B. Y. and I. Sezai (2002). Numerical simulation of three-dimensional laminar multiple impinging square jets. *International Journal of Heat and Fluid Flow* 23, 509-518.

Armaly, B. F., F. Durst, J. C. F. Pereira and B. Schonung (1983) Experimental and theoretical investigation of backward-facing step flow. *Journal of Fluid Mechanics* 127, 473-496.

Arquis, E., M. A. Rady and S. A. A. Nada (2006) numerical investigation and parametric study of cooling an array of multiple protruding heat sources by a laminar slot air jet. *International journal of heat and fluid flow* 28, 788-805.

Buchlin, J. M. (2011). Convective Heat Transfer in Impinging- Gas- Jet Arrangements. *Journal of Applied Fluid Mechanics* 4(2), 137-149.

Buddhika, N. H. (2009). A numerical study of heat transfer performance of oscillatory impinging jets. *International Journal of Heat and Mass Transfer* 52 396-406.

Bula, A. J. and M. M. Rahman (2000). Numerical modeling of conjugate heat transfer during impingement of free liquid jet issuing from a slot nozzle *International Journal of Heat and*

Mass Tran. 38, 45-66.

Chiriac, V. A. and A. Ortega (2002). A numerical study of the unsteady flow and heat transfer in a transitional confined slot jet impinging on an isothermal surface. *International Journal of Heat and Mass Transfer* 45, 1237-1248.

Dae, H. L., J. R. Bae, H. J. Park and J. S. Lee (2011). Phil Ligrani Confined, milliscale unsteady laminar impinging jet and surface Nusselt numbers *International Journal of Heat and Fluid Flow* 54, 2408-2418.

David, S. C., P. Rajesh kanna, G. R. Madhusudhana, P. Venkumar and h. Mohammed (2012). Numerical investigation of heat transfer from a two-dimensional sudden expansion flow using nanofluids. *Numerical Heat Transfer, part A* 61, 527-546.

David, S. C., G. R. Madhusudhana, P. Venkumar, P. Rajesh Kanna and H. A. Mohammed (2012). Numerical Investigation on Laminar Forced Convection Flow Due to Sudden Expansion Using Nanofluids. *Journal of Computational and Theoretical Nanoscience* 9, 1-11.

Dipankar, S., M. A. R. Sharif (2004). Numerical modeling of slot-jet impingement cooling of a constant heat flux surface confined by a parallel wall. *International Journal of Thermal Sciences* 43 877-887.

Ertan, B. (1999). Confined impinging air jet at low Reynolds numbers. *Experimental Thermal and Fluid Science* 19 27-33.

Farial, A. J., R. T. Graham and Ozden F Turan, Flow Visualization and Heat Transfer Characteristics of Liquid Jet Impingement. *International Journal for Computational Methods in Engineering Science and Mechanics* 13, 239-253.

Hee, J. P., K. a. Kumar, A. S. Mujumdar (2005). Heat transfer from a pulsed laminar impinging jet. *International Communications in Heat and Mass Transfer* 32, 1317-1324.

Ihsan, D., H. I. Dagtekin and H. F. Oztop (2008). Heat transfer due to double laminar slot jets impingement onto an isothermal wall within one side closed long duct. *International Communications in Heat and Mass Transfer* 35, 65-75.

Jambunathan, L. M. and A. Button (1992). Review of heat transfer data for single circular jet impingement. *International journal of heat and fluid flow* 12, 106-115.

Kazuyoshinakabe, E., F. Jens, Y. Eschenbacher, T. Yamamoto and K. Suzuki (2001). Interactions of longitudinal vortices generated by twin inclined jets and enhancement of impingement heat transfer. *International journal of heat and fluid flow* 22, 287-292.

Liu Haiyong, B., Q. Hongfua, L. Songlingb and L. Cunliang (2011). Flow Field Investigation in a

- Trapezoidal Duct with Swirl Flow Induced by Impingement Jets. *Chinese Journal of Aeronautics* 24 8-17.
- Lytle, D. and B. W. Webb (1994). Air jet impingement heat transfer at low nozzle-plate spacings. *International Journal of Heat and Mass Transfer* 37, 1687–1697.
- Muthukannan, M., P. Rajeshkanna, A. Bajpai and S. Jeyakumar (2014). Numerical Investigation On The Fluid Flow Characteristics Of A Laminar Slot Jet On Solid Block Mounted On A Horizontal Surface. *Arabian Journal of Science and Engineering*. 39, 8077–8098.
- Patankar, N. (1980). *Heat Transfer and Fluid Flow*, Hemisphere London 113-134.
- Peng, W., J. Lva, M. Baia, Y. Wanga and Ch. Hua (2014). Numerical investigation of the flow and heat behaviours of an impinging jet. *International Journal of Computational Fluid Dynamics* 1-15.
- Promvongse, S., S. Sripattanapipat, a. Tamna, S. Kwankaomeng and C. Thianpong (2010). Numerical investigation of laminar heat transfer in a square channel with 45° inclined baffles. *International Communications in Heat and Mass Transfer* 37, 170–177.
- Rajesh, K. and M. Kumar Das (2005). Conjugate forced convection heat transfer from a flat plate by laminar plane wall jet flow. *International Journal of Heat and Mass Transfer* 48, 2896–2910.
- Rajesh, K. and M. Kumar Das (2006). A short note on the reattachment length for BFS problem. *International Journal for Numerical Methods in Fluids* 50, 683–692.
- Rajesh Kanna, P. and M. Kumar Das (2006). Numerical Simulation of Two-Dimensional laminar incompressible wall jet flow under backward-facing step. *Journal of Fluids Engineering* 128 1023-1035.
- Sami, A. S. (1992). A numerical study of the flow and heat transfer characteristics of an impinging laminar slot-jet including crossflow effects. *International Journal of Heat and Mass Transfer*, 35, 2501-2513.
- Sivasamy, A., V. Selladurai and P. Rajeshkanna (2007). Numerical simulation of two-dimensional laminar slot-jet impingement flows confined by a parallel wall. *International journal for Numerical Methods in Fluids* 55, 965–983.
- Sivasamy, A., V. Selladurai and P. Rajeshkanna (2008). Heat Transfer Study of 2D laminar incompressible confined impinging slot jet flow. *International Conferences on Advances in Mechanical Engineering* 1-3.
- Sparrow, E. M. and T. C. Wong (1975). Impingement transfer coefficients due to initially laminar slot jets. *International Journal of Heat and Mass Transfer* 8, 597–605.
- Tesar, V. and J. Barker (2002). Dominant Vortices in Impinging Jet Flows. *Journal of Visualization* 5 121-128.